Techniques for measuring the elastic wave velocities of melts and partial molten systems under high pressure conditions

Hans J. Mueller, Kerstin Roetzler[1], Frank R. Schilling[2], Christian Lathe, Michael Wehber

GFZ German Research Centre for Geosciences, Telegraphenberg, D-14473 Potsdam, Germany

[1] formerly at GFZ

[2] University of Karlsruhe, Geologisches Institut, D-76128 Karlsruhe, Germany

Abstract

The Earth's deep interior is only accessible by indirect methods, first and foremost seismological studies. The interpretation of these seismic data and the corresponding numerical modelling requires measurements of the elastic properties of representative Earth materials under experimental simulated in situ conditions. Different techniques and results for experiments under crustal and mantle conditions are described.

Keywords: A. ceramics, C: high pressure, C. X-ray diffraction, D. elastic properties, D. phase transitions

1 Introduction

Models of the Earth's interior are essentially based on seismic measurements because these data supply a much more detailed image than any other geophysical or geochemical method. Recent geophysics is presenting exciting new seismic tomography data and corresponding numerical models implying that under suitable conditions subducting slabs can reach the core mantle boundary (CMB) (van der Hilst, 1995; Lowman and Jarvis, 1993, 1995, 1996, 1999; Peacock et al., 1994; van der Hilst and Karason, 1999). Furthermore using short- and long-period precursors of PKP phases ultra-low velocity zones (ULVZ) at the core-mantle boundary beneath the Western Pacific (Wen and Helmberger, 1998) and central Africa (Ni and Helmberger, 2001) were observed. In spite of resolving problems there is a rising indication for a relation of the base

of superplumes to these thermo-chemical piles (Kellogg et al., 1999; Romanowicz and Gung, 2002; Lassak et al., 2007). Despite all enigmatic details there is no doubt that even at the CMB really nothing is simple and stratified as previously thought, i.e. through the whole mantle we probably have rocks of at least similar complexity than at crustal depths. For high pressure research aimed to geophysics that means there is a demand for a petrophysics and petrology of the mantle and the elastic properties of complex mineral assemblages, i.e. some kind of rock, under the conditions of more or less partial melting at deep Earth's conditions is a key question.

2 Experimental Techniques

2.1. Gas Pressure Systems

For petrophysical measurements crustal conditions (about 1.2 GPa / 520 to 700˚C) can be experimentally simulated by oil pressure vessels, gas pressure systems and piston-cylinder apparatus. The hydrostatic systems (oil and gas pressure) ensure a stress-free sample. Gas as pressure transmitting medium makes temperatures higher than 1000˚C accessible, but require safety precautions because of the high energy capacity of compressed gases (Manghnani et al., 1974). Using noble gases inhibit chemical reactions with sample and sensors (Mueller, 1995; Mueller and Raab, 1995, 1997; Mueller et al., 2002). The common use of argon limits the maximum pressure to about 1,3 GPa because of freezing. Getting developed an argon pressure system with the peak pressure of 6 GPa keeping the gas frozen at the sealings but gaseous around the sample by the heater (Getting, and Spetzler, 1993; Getting and Burnley, 1994). We used a high performance gas pressure vessel (Fig. 1) using helium able to simulate the conditions through the whole crust down to the uppermost mantle up to about 80 km depth. The maximum conditions are 2.5 GPa and 1600˚C (Mueller and Massonne, 2001).

2.1.1. Ultrasonic travel time measurement

Figure 2 shows a scheme of 2 typical setups for encapsulated samples. The ultrasonic waves are produced and detected by piezoelectric transducers. Because of the high temperature resistance lithium niobate is the optimum material choice. Triple mode transducers generate compressional, shear waves and a useless mixed mode simultaneously (Mueller et al., 2007; Ishikawa et al., 2009). If the energy level of these transducers is not sufficient because of highly attenuating samples separate pairs of single mode transducers has to be used. Because the melting temperature of rocks exceeds the Curie temperature of lithium niobate of about 500˚C ceramic buffer rods are used to keep the transducers cooler than the sample. To measure the elastic wave velocities the travel time of a pulse is measured resulting in an uncertainty of 1 to 2 %. The frequency of the ultrasonic waves is 1 MHz corresponding to a wavelength of about 7 mm inside the rock sample. To limit energy loss by scattering the wavelength has to be greater than the mineral grain size of the rock sample.

2.1.2. Set-up and Results

Fig. 3 shows the elastic wave velocity data for p- and s-waves, as well as the Poisson's ratio as a function of pressure at normal temperature and as a function of temperature up to 1,200˚C at 0.5 GPa pressure for 3 different Saxonian Erzgebirge granites. Disregarding minor differences all samples have (1) a greater velocity increase in v_p than in v_s up to about 0.1 GPa pressure, (2) a more or less pressure independent Poisson's ratio except for pressures below 0.05 GPa, (3) more or less temperature independent v_p, v_s, and Poisson's ratio up to 550˚C at 0.5 GPa pressure, (4) a strong decrease of v_p and v_s between 550˚C and 1,200˚C, and (5) a corresponding increase of the Poisson's ratio at the same temperature range approaching the value of 0.5 for an ideal fluid. Looking in more detail the whole process can be divided in 6 stages:

Stage I: Crack closing

In dependence on rock's structure, crack distribution, and grain boundary coverage by thin mineral layers it finished somewhere between 0.2 and 0.5 GPa.

Stage II: Pressure shift of elastic moduli

It is characterized by proportionally increasing velocities and constant or slightly increasing Poisson's ratio.

Stage III: Temperature shift of elastic moduli

There is the opposite tendency than in stage II.

Stage IV: Thermal cracking overlapped by the quartz α-β transition in quartz bearing rocks and start of mineral dehydration, i.e. disintegration of micas.

Stage V: Beginning of partial melting

The local onset of fluid induced partial melting is indicated by an increasing Poisson's ratio because the intergranular melt films affect v_p more distinctive than v_s.

Stage VI: Massive partial melting

At higher temperatures the velocity curves approach linear behaviour again as the increasing amount of melt starts to form tracks and bodies of larger scale with less influence on the velocities.

To learn the relation between structural development under the influence of pressure and temperature during the experiments and the corresponding elastic wave velocity data after the runs thin sections of the samples were microscopically analyzed, see Fig. 4. As an example Fig. 5 show a microsection of a granite with melt margins, the corresponding binary picture made by digital image processing, as well as the orientation distribution of these melt margins. This technique provides a quantitative analysis of the structural development during the experimental runs. To get information from previous stages additional experiments quenched at earlier stages

of the process were performed. Fig. 6 demonstrates the results for granite Ki1. Between 750˚C and 800˚C at 0.5 Gpa pressure the total melt content increases from 2% to 6%. But this is not only a quantitative effect, but also a qualitative one. The main orientation of melt margin's long "particle" axes turns from 350˚ to 355˚. This is accompanied by a stronger alignment, i.e. secondary orientations become less important. The development of granulite exposed to 1.5 GPa pressure in a long-term experiment of 48 h duration is totally contrary, see Fig. 7. Between 750˚C and 800˚C the melt content increases from 18% to 36%. Contrary to granite the orientation distribution of the melt margins developes from a more or less uniform orientation around 0˚ to more or less even significant 3 orientations at 5˚, 20˚, and 120˚. Considering the high total melt content of 36% this result is surprizing at the first glance. It makes clear how important the "memory" of a rock is for its further development. Granulite is highly preferred orientated, granite is not. Results of this type are nor only interesting for crustal research. Establishing the deep mantle petrophysics and petrology as derived above we have to make the corresponding artificial rocks of strange mineralogy, not at any time any geologist saw, in a representative way. A detailed quantitative knowledge about the relation between structure and physical properties in natural rocks is indispensable for doing that realistically.

Fig. 8 compares theoretical data from Mavko, 1980 with our experimental data for v_p and v_s. The experiments verify the theory. Small melt contents up to about 3% are exclusively located in thin layers (f - for foils); higher amounts create more and more spacy melt bodies (f+t - for foils and tubes) approaching a stage where this layers diminish (t - for tubes).

Contrary to the classical petrological imagination making mineral reactions in natural rocks fast enough for experiments require powdering or making gels from oxide mixtures we found structural creation processes in unprocessed natural rocks during long-term petrophysical experiments. Fig. 9 shows an overview of a granulite microsection exposed to 1.5 GPa pressure and 800˚C for 48 h, as well as a magnified detail. A garnet from the original rock is going to

decompose and is surrounded frm small garnets newly formed from the melt during the experiment. The differentiation is not only visually, but also based on a slightly different chemistry. The new formed garnets and orthopyroxenes are rich in iron and magnesium from molten micas. We also found new formed corundum needles of about 30 µm lenth, see Fig. 10. The melting reactions are as follows:

ms + qtz + V = L (720˚C, 1.5 GPa)

ms + plg + qtz + ky = bt + kfs (new) + ky + L (780˚C, 1.5 GPa)

bt + plg - qtz + ky = gnt (new) + kfs (new) + L (800˚C, 1.5 GPa)

plg + qtz + ky = gnt (new) + kfs (new) + L (800˚C, 1.5 GPa)

bt + qtz = opx (new) + kfs (new) + L (800˚C, 1.5 GPa)

new formed gnt and opx are rich in Fe and Mg from micas

2.2. Multi-anvil systems

The experimental simulation of transition zone and deep mantle conditions require quasihydrostatic pressure generation. In principle 3 techniques exist: Paris-Edinburgh cell, multi-anvil devices (MA), and diamond anvil cells (DAC), see Fig. 11. The Paris-Edinburgh cell is popular because it is very simple and small, i.e. it can be used as an additional option at beam lines designed for DACs. The sample size is quite big (about 80 mm^3), but the pressure is normally limited to less than 10 GPa corresponding about 300 km depth. Using sintered diamond anvils peak pressures of 25 GPa were published. In principle DACs follow the same basic concept - pushing 2 anvils together, but the anvils are single-crystal diamonds. Peak pressures of 300 GPa to even 500 GPa were published, but the sample size of 10^{-11} to 10^{-14} m^3 is minor. Laser heating results in huge temperature gradients inside the sample. Resistance heating is unable to produce the temperatures of 5,000˚C to 6,0000˚C coresponding to the inner core representing

pressures. Contrary to the first mentioned techniques MAs, also called Large Volume Presses (LVP), have a 3-dimensional pressure generation in principle because hydraulically driven 6 or more anvils are pushed synchronistically towards the sample. The sample volume is 10^{-7} to 10^{-8} m^3, i.e. it is thousand to 10-million-fold bigger than that in DACs. The pressure limits are about 12 GPa for single-stage apparatus and about 35 GPa for double-stage apparatus (Mueller et al., 2006). Using sintered diamond anvils at the second stage peak pressures of 80 GPa were published (Tange et al., 2008). The temperature is limited to about 2,300˚C. We used the single-stage DIA MAX 80 (300 tons) and the double-stge DIA MAX 200x (1750 tons) (see Fig. 12) installed at HASYLAB beamlines F 2.1 and W II at DESY, Hamburg, Germany for our experiments.

2.2.1. Ultrasonic interferometry

Contrary to the gas pressure system using the travel time technique is not reasonable. The distance between transducer and sample is much longer than the sample. Additionally very often the travel path is composed of multiple parts. All that would reduce the accuracy of the measurement to 10% or worse. Ultrasonic interferometry evaluates the superposition of the elastic waves reflected from the front and rear face of the sample. The result is a periodical sequence of constructive and destructive interferences (McSkimin, 1950; Li et al., 1995; Mueller et al., 2002, 2003, 2005a). For known sample length the elastic wave velocity can be calculated from the (frequency) distance between the maxima or minima in the interference pattern. That means the sample length under in situ conditions is strongly needed, i.e. precise high pressure ultrasonic interferometry require X-radiography at a light source (Fig. 13). The practical uncertainty of the interferometric technique used in LVPs is in the range of 0.2%, i.e. 10-times better than the travel time method and totally independent on the length of the entire travel path

in particular. But there is a problem with classical ultrasonic interferometry, it is very time consuming. Sweeping through the frequency range of several tens of MHz costs about 30 minutes, much too long for transient measurements. The data transfer function (DTF) (Li et al, 2002; Mueller et al., 2005b) technique sends a calculated signal to the transducer comprising the entire frequency range, which was used by the classical sweep technique (Fig. 14). Consequently the reply of the system also comprises all the superpositions of the elastic waves reflected from both front faces of the sample. The superposition pattern of the classical sweep technique is recaptured by a post-experimental convolution. So, the syn-experimental time and effort of the frequency sweep is shifted to a post-experimental calculation. Saving the highly resoluted transfer function to a PC-harddrive costs about 1 minute.

2.2.2. Set-up and Results

Measuring the elastic wave velocities of melts under simulated mantle conditions require some refinement of the set-up design. First of all the sample has to be encapsulated to prevent the melt from leaking out of the working section resulting in a blow-out of the whole set-up. With a molten sample the alignment of buffer and reflector becomes critical. Otherwise the reflected waves from the front and rear face of the sample would be no longer parallel to each other resulting in problems with the evaluation of their superposition. The high melting temperatures of basic rocks result in softening of the carrier materials for the set-ups accompanied by an increased blow-out hazard. Classical capsule materials used in experimental petrology - gold and platinum - drop out of the choice because of their high X-ray density. Even a thin metal sheet between buffer and sample for its encapsulation is a problem because of the short ultrasonic wave length of several tens of micrometers.

We designed a set-up with an encapsulation made from titanium covering the entire travel path including reflector and blow-out preventer (Fig. 15). It is sealed during the first stages of the

high pressure run, ensures the alignment of the working section, and is sufficiently X-ray transparent. For the first test runs we picked a material with a low melting point, but a very low viscosity - thermo-plastical lute. Any leaking or misalignment of the molten sample could not be observed. Fig. 16 shows the elastic wave velocity results up to 0.5 GPa pressure and 400˚C temperature. Fig. 17 displays the X-radiographs taken before and after sample melting.

3. Triple-stage systems

There is a gap between the range of operation of LVPs and DACs. From geophysical point of view recent results on ultra-low velocity zones above the core-mantle boundary are the most outstanding task for present day mineral physics. The fundamental phase transitions in that range of conditions are known from DAC experiments. For a comprehensive understanding of processes in complex mineral systems single crystal measurements with micrometer-sized samples are surely insufficient. Utsumi et al., 1986 published a technique to reach 60 GPa using sintered diamond anvils as additional stage in a single-stage DIA-type LVP. Wang and Utsumi, 2005 reported the further pressure increase by using deformation DIA systems. We performed triple-stage experiments using TC-anvils (Fig. 18) and could reach nearly 50 GPa (Mueller et al., 2006). Using HIME-diamond (nano-polycrystalline diamond) the Irifune group published a peak pressure of more than 90 GPa (Kunimoto and Irifune, 2006) and reached nearly 100 GPa (pers. comm.) recently.

4. Summary and future prospects

We presented designs for measuring the elastic wave velocities of melts and partial molten systems under high pressure conditions and their results. Depending on the maximum pressures different techniques have to be used for the experimental simulation of deep crustal to uppermost mantle- and deep mantle conditions. Many challenges still exist. One of the most important one

with the most far-ranging general meaning for our understanding of the dynamics of the deep Earth seems to be the material / structural interpretation of the ultra-low velocity regions above the core-mantle boundary.The conditions of the core mantle boundary - about 140 GPa and more than 2,000˚C - are not accessible for recent LVPs. Triple-stage techniques are a promising way to simulate these conditions in a volume sufficient to investigate the processes in complex mineral assemblages under these extreme conditions.

Acknowledgments: We would like to express our special thanks to the editor H. Couvy for patience and kind guidance which was essential for the preparation of the manuscript. We would like to acknowledge very fruitful discussions with B. Li, Y. Wang, T. Irifune, and H.-J. Massonne. The authors are particularly indebted to D. Frost, M. Koch-Müller, and M. Spiwek for technical support, as well as M. Kreplin, R. Sünkel, and W. Steiner for their firm involvement in special preparation.

References

1. R.D. Van der Hilst, Complex morphology of subducted lithosphere in the mantle beneath the Tonga trench, Nature, v. 374 (1995), 154-157.

2. J.P. Lowman, G.T. Jarvis, Mantle convection flow reversals due to continental collisions, Geophys. Res. Lett., Vol. 20 (1993), 2087-2090.

3. J.P. Lowman, G.T. Jarvis, Mantle convection models of continental collisions and breakup incorporating finite thickness plates, Phys. Earth Planet. Int., Vol. 88 (1995), 53-68.

4. J.P. Lowman, G.T. Jarvis, Continental collisions in wide aspect ratio and high Rayleigh number two-dimensional mantle convection models, J. Geophys. Res., Vol. 101 (1996), 25,485-25,497.

5. J.P. Lowman, G.T. Jarvis, Effects of mantle heat source distribution on continental stability, J. Geophys. Res., Vol. 104 (1999), 12,733-12,746.

6. S:M. Peacock, T. Rushmer, and A.B. Thompson, Partial melting of subducting oceanic crust, Earth Planet. Sci. Lett., 121 (1994), 127-244.

7. R.D. Van der Hilst, R.D., H.Kárason, Compositional heterogeneity in the bottom 1000 km of Earth's mantle: towards a hybrid convection model, Science, v. 283 (1999), 1885-1888.

8. L. Wen, D.V. Helmberger, Ultra-low velocity zones near the core-mantle boundary from broadband PKP precursors, Science, vo. 279, no. 5357 (1998), 1701-1703.

9. S. Ni, S., D. V. Helmberger, Probing an ultra-low velocity zone at the core mantle boundary with P and S waves, Geophys. Res. Lett., 28 (12) (2001), 2345–2348.

10. L. H. Kellogg, B.H. Hager, and R. D. van der Hilst, Compositional Stratification in the Deep Mantle, Science, vol. 283, no. 5409 (1999), 1881-1884.

11. B. Romanowicz, Y. C. Gung, Superplumes from the core-mantle boundary to the base of the lithosphere, Science,296 (2002), 513-516.

12. T.M. Lassak, A.K. McNamara, and S. Zhong, Influence of thermochemical piles on stress

development at Earth's core-mantle boundary, Earth Planet Sci. Lett., 261 (2007), 443-455.

13. M.H. Manghnani, R. Ramananantoandro, and S.P. Clark, Compressional and shear wave velocities in granulite facies rocks and eclogites to 10 kbar, J. Geophys. Res., 79 (1974), 5427-5446.

14. H.J. Mueller, Modelling the lower crust by simualtion of the in situ conditions: an example from the Saxonian Erzgebirge, Phys. Earth Plan. Int., 92 (1995), 3-15.

15. H.J. Mueller, S. Raab, The velocities of elastic P- and S-wavesin high-grade metamorphic rocks under high pressures and temperatures; Geophys. J., 17 (1997), 78-85.

16. H.J. Mueller; S. Raab, Elastic wave velocities of granite at experimental simulated partial melting conditions, Phys. Chem. Earth, 22 (1995), 93-96.

17. H.J. Mueller, F.R. Schilling, and J. Lauterjung, In-situ investigation of physical properties of rocks and minerals at lower crustal and mantle conditions - methods, measurements, challenges, Z. Geol. Wiss., 30 (1/) (2002), 1-28.

18. I.C. Getting, H.A. Spetzler, Gas-charged piston-cylinder apparatus for pressures to 4 GPa, Eos, Trans. Am. Geophys. Union, 60 (18) (1993), F317.

19. I.C. Getting, P.C. Burnley, Absolute pressure and temperature calibration to 6 GPa and 1,700 K, Eos, Trans. Am. Geophys. Union, 75 (44) (1994), F722.

20. H.J. Mueller, H.-J. Massonne, Experimental high pressure investigation of partial melting in natural rocks and their influence on V_p and V_s, Phys, Chem. Earth (A), vol. 26 (2001), 325-332.

21. H.J. Mueller, F.R. Schilling, and C. Lathe, Multianvil techniques in conjunction with synchrotron radiation at Deutsches Elektronen Synchrotron (DESY) - Hamburger Synchrotron LABor (HASYLAB), Geol. Soc. Am, Special Paper 421 (2007), 207-226.

22. M. Ishikawa; Y. Matsumoto, and M. Arima, Simultaneous measurements of compressional wave and shear wave velocities, Poisson's ratio, Vp/ Vs under deep crustal pressure and temperature conditions: Example of silicified pelitic schist from Ryoke belt SW Japan, Island Arc

(2009), in press.

23. G. M. Mavko, Velocity and attenuation in partially molten rocks, J. Geohys. Res., 85 (B10) (1980), 6,983-6,990.

24. H.J. Mueller, F.R. Schilling, C. Lathe, and J. Lauterjung, Recent development of experimental techniques for high-pressure mineral physics under simulated mantle conditions, High Press. Res., vol. 26 (no. 4) (2006), 529-537.

25. Y. Tange, T. Irifune, and K.-I. Funakoshi, Pressure generation to 80 GPa using multianvil apparatus with sintered diamond anvils, High Press. Res., vol. 28 (3) (2008), 245-254.

26. H.J. McSkimin, (1950): Ultrasonic measurement techniques applicable to small solid specimens. J. Acoust. Soc. Am., vol. 22 (1950), 413-418.

27. B. Li, R.C. Liebermann, G.D. Gwanmesia, and I. Jackson, Elastic wave velocities of mantle minerals to 10 GPa in multi-anvil apparatus by *in situ* ultrasonic techniques, Eos Trans. AGU, vol. 76 (1995), 277.

28. H.J. Mueller, J. Lauterjung, F.R. Schilling, C. Lathe, and G. Nover, Symmetric and asymmetric interferometric method for ultrasonic compressional and shear wave velocity measurements in piston-cylinder and multi-anvil high-pressure apparatus. Jur. J. Mineral. 14 (2002), 581-589.

29. H.J. Mueller, F.R. Schilling, J. Lauterjung, and C. Lathe, A standard free pressure calibration using simultaneous XRD and elastic property measurements in a multi-anvil device. Eur. J. Mineral. 15 (2003), 865-873.

30. H.J. Mueller, C. Lathe, and F.R. Schilling, Simultaneous determination of elastic and structural properties under simulated mantle conditions using multi-anvil device MAX80, in: J.

31. Chen, Y. Wang, T. Duffy, G. Shen, and L. Dobrzhinetskaya, (Eds.), Advances in High Pressure Technology for Geophysical Application, chapter 4, Elsevier B.V., London/Amsterdam/New York, 2005a, 67-94.

32. B. Li, K. Chen, J. Kung, R.C. Liebermann, and D. Weidner, Sound velocity measurement using transfer function method, J. Phys. Condens. Matter, vol. 14 (2002), 11,337-11,342.

33. H.J. Mueller, F.R. Schilling, C. Lathe, and J.Lauterjung, Calibration based on a primary pressure scale in a multi-anvil device, (Eds.), Advances in High Pressure Technology for Geophysical Application, chapter 21, Elsevier B.V., London/Amsterdam/New York, 2005b, 427-449.

34. W. Utsumi, N. Toyama, S. Endo, F.E. Fujita, and O. Shimomura, X-ray diffraction under ultrahigh pressure generated with sintered diamond anvils, J. Appl. Phys, vol. 60 (1986), 2201-2204.

35. Y. Wang, W. Utsumi, 6/2: A possible marriage between multi-anvil and DAC. (oral paper), COMPRES Annual Meeting 2005, Mohonk Mountain House, New Paltz, June 16-19, pers. comm.

36. T. Kunimoto, T. Irifune, Generation of ultra-high pressure in a triple stage multi-anvil (6-8-2) system, Eos, Trans. Am. Geophys. Union, (2006), MR11A-0089.

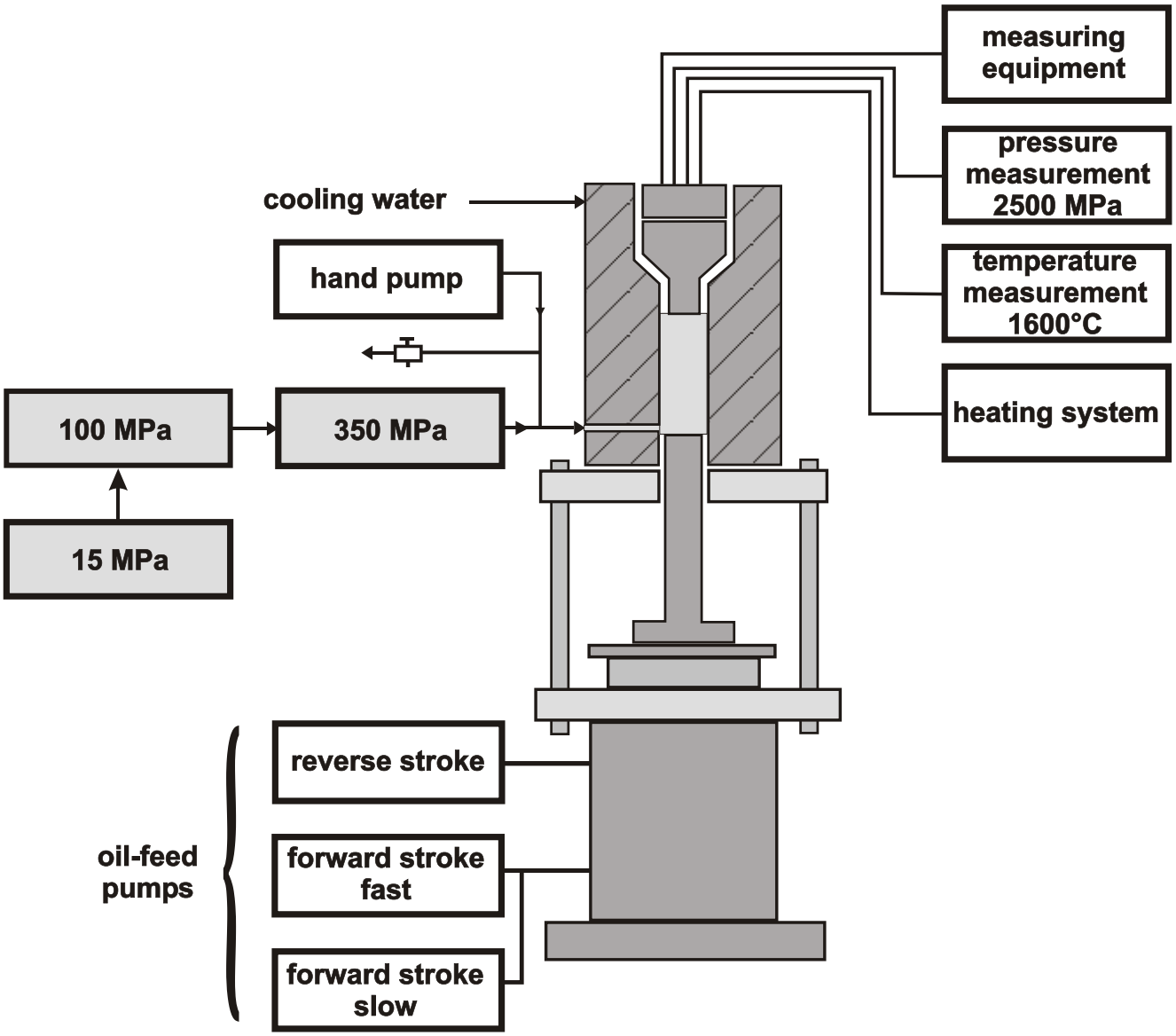

Fig. 1: Scheme of the high performance gas apparatus with a maximum pressure of 2.5 GPa

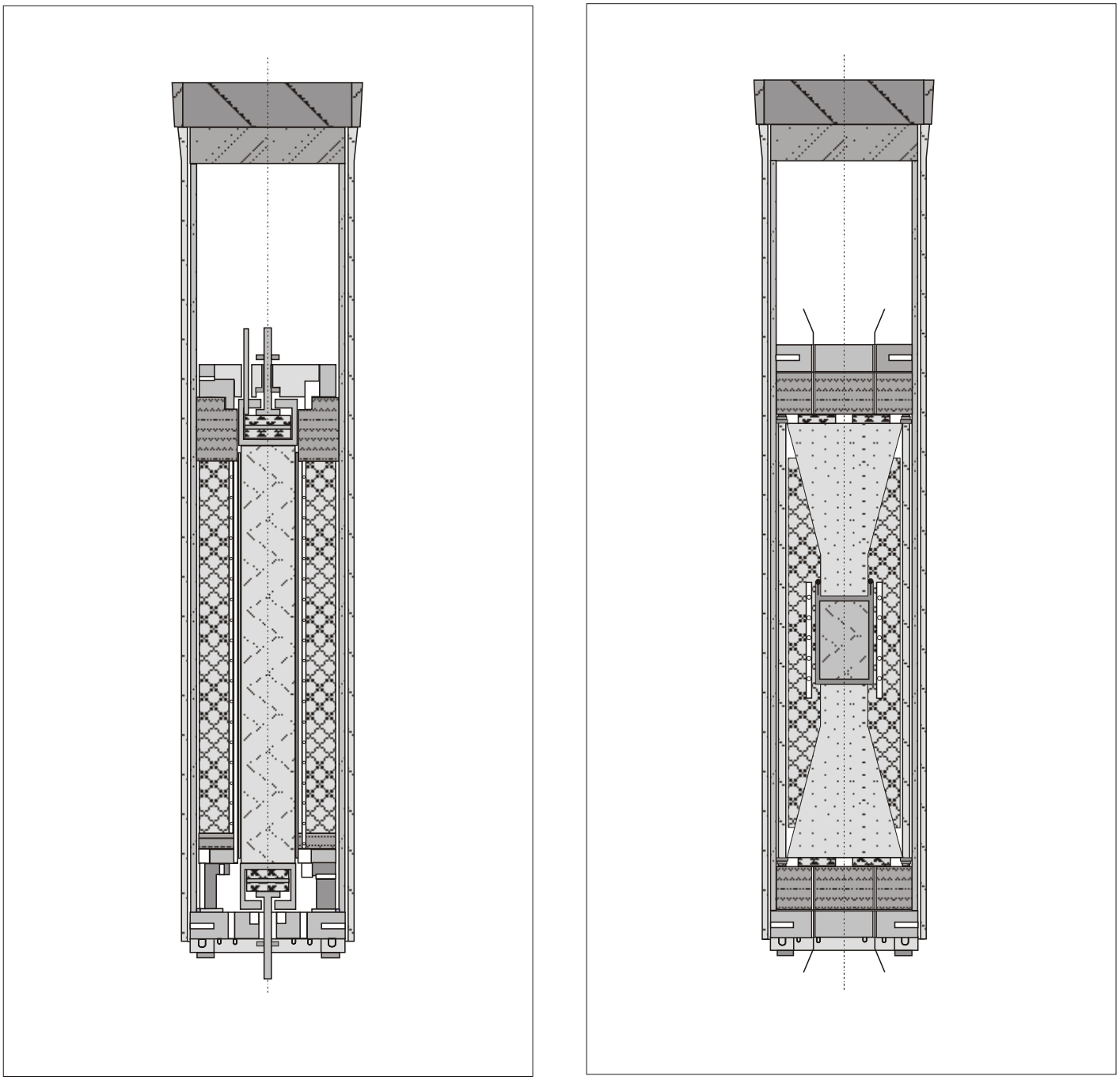

Fig. 2: Internal set-up with different sample encapsulation versions and parallel or stacked transducers for v_p and v_s

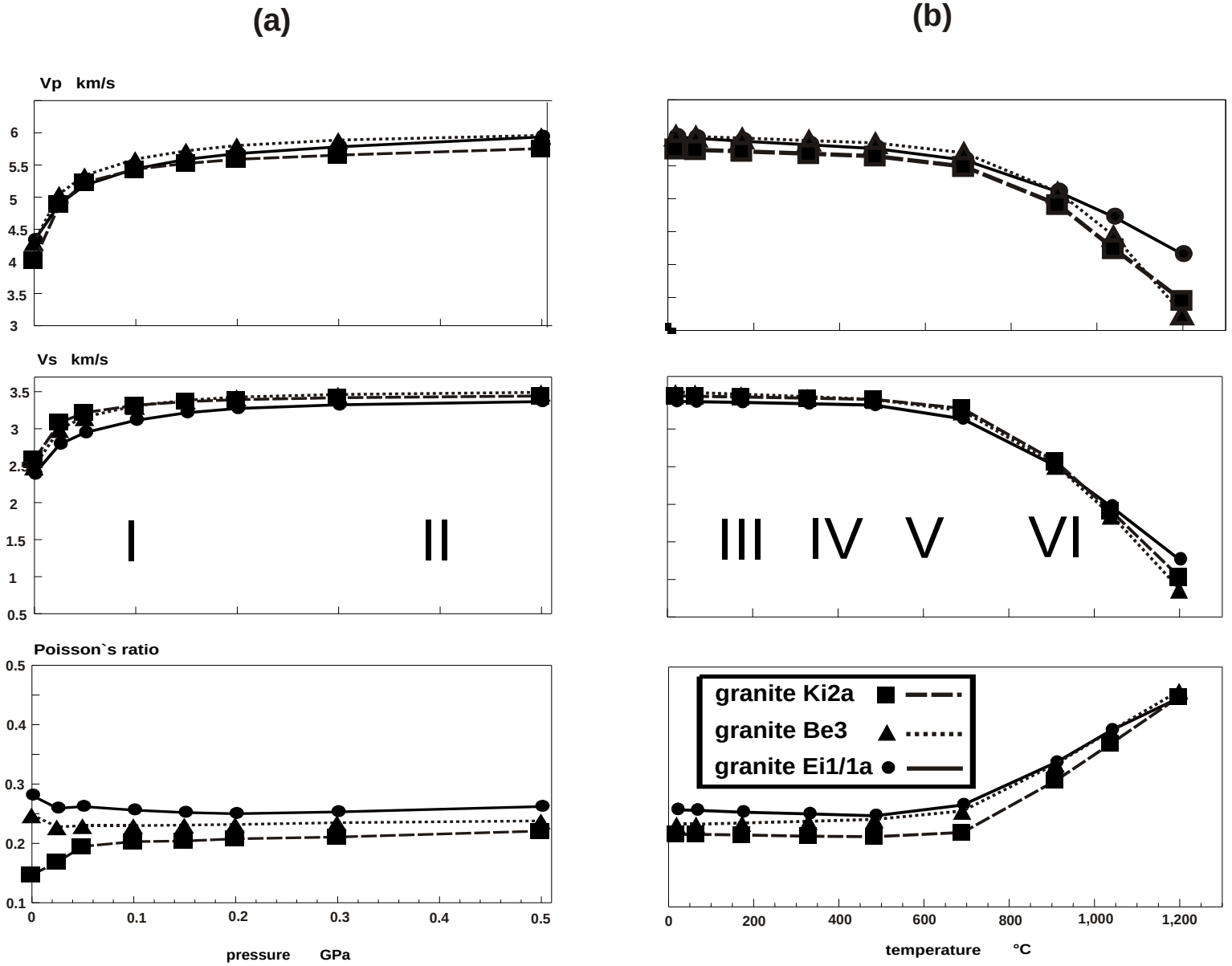

Fig. 3: v_p and v_s for different Saxonian Erzgebirge granites up to 0.5 Gpa and 1,200°C

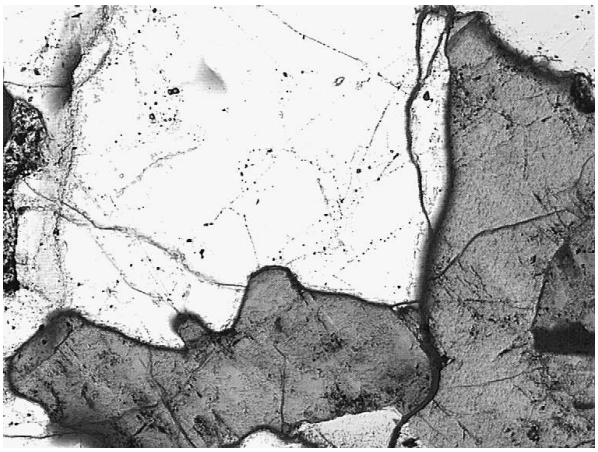

2% melt at 690°C

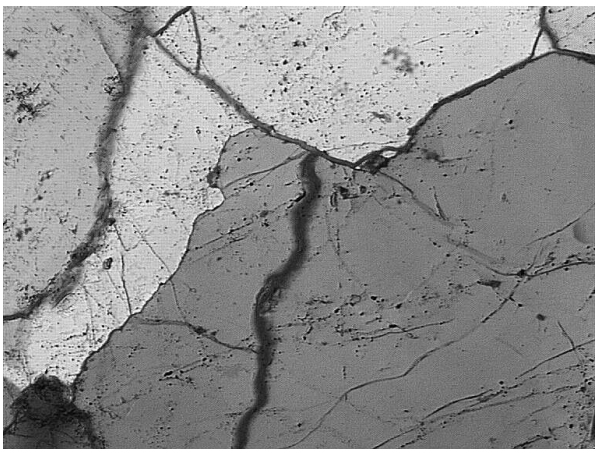

4% melt at 910°C

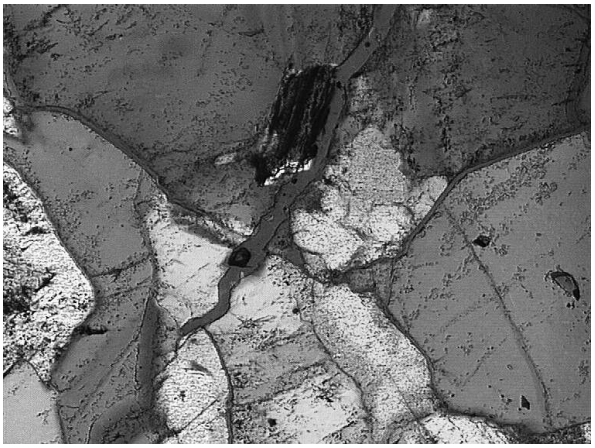

10% melt at 1,040°C

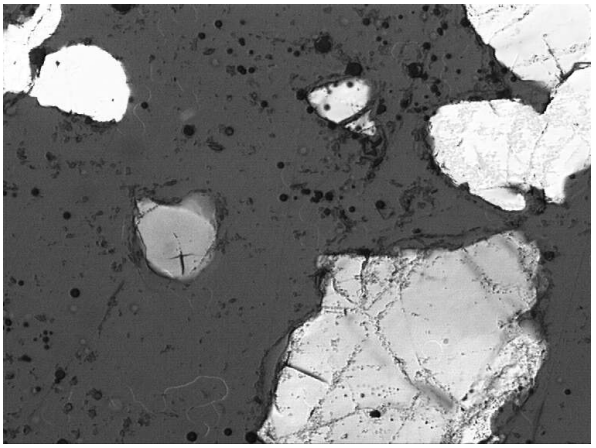

61% melt at 1,200°C

Fig. 4: Melt content and melt distribution as function of Temperature at 0.5 GPa pressure

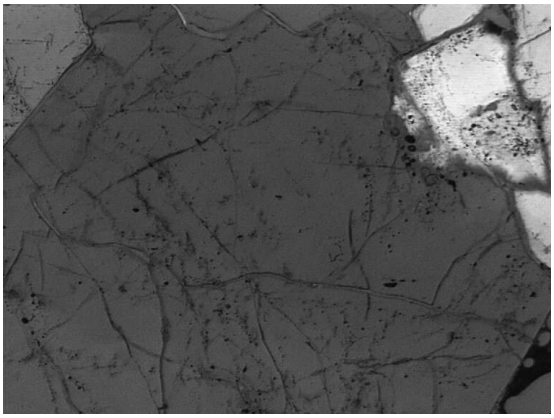

microsection image

binary picture of melt margins

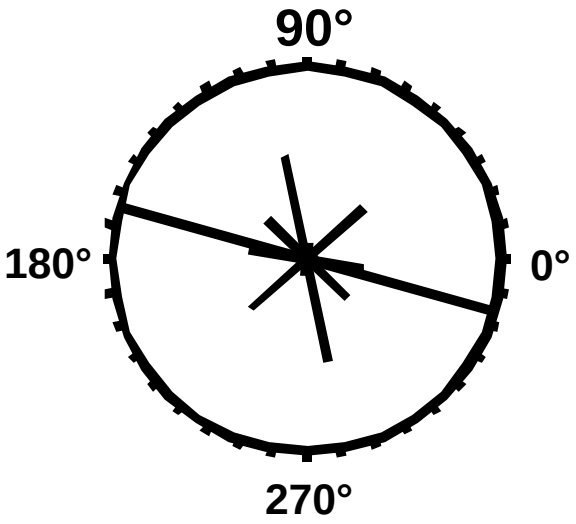

orientation distribution
of
melt margin‘s
long „particle“ axes

Fig. 5: Microsection image of a partial molten granite sample, the corresponding binary picture made by digital image processing, and calculated orientation distribution of melt margins

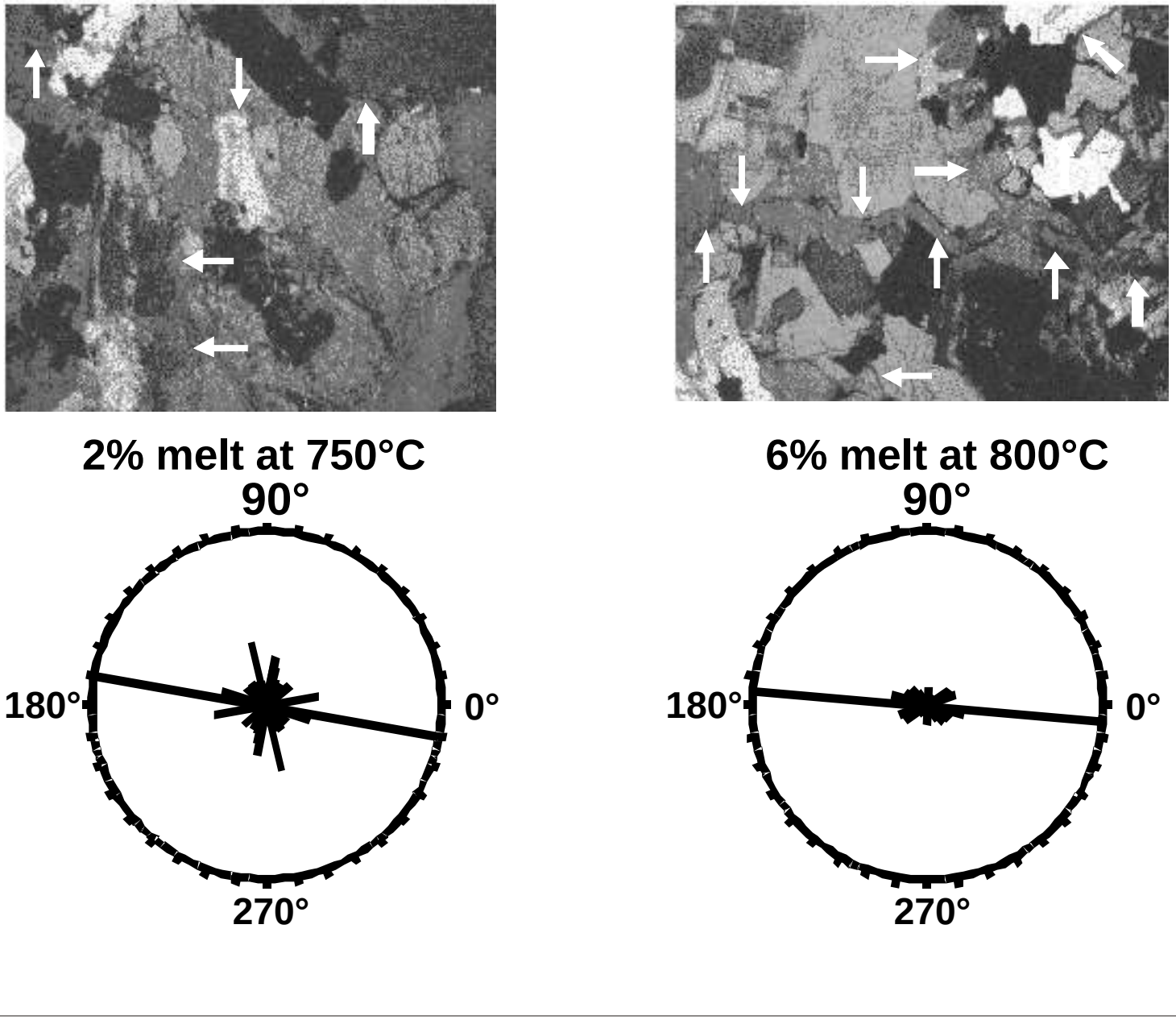

Fig. 6: Petrofabric analysis of Erzgebirge granite Ki1 at 0.5 GPa pressure
- orientation distribution of melt margins

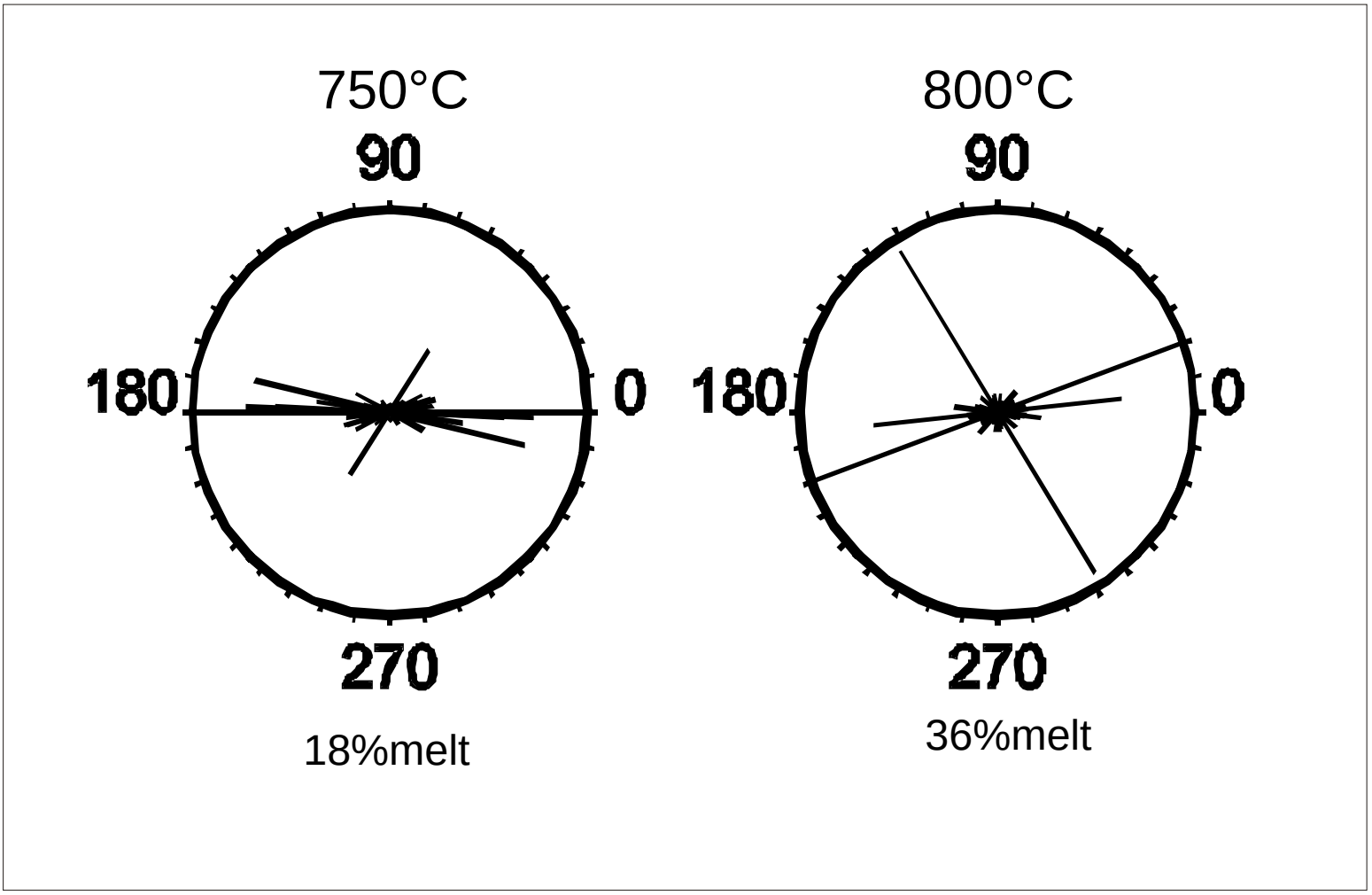

Fig. 7: Orientation distribution of melt margins for Erzgebirge granulite at 1.5 Gpa and 48 h temperature exposition

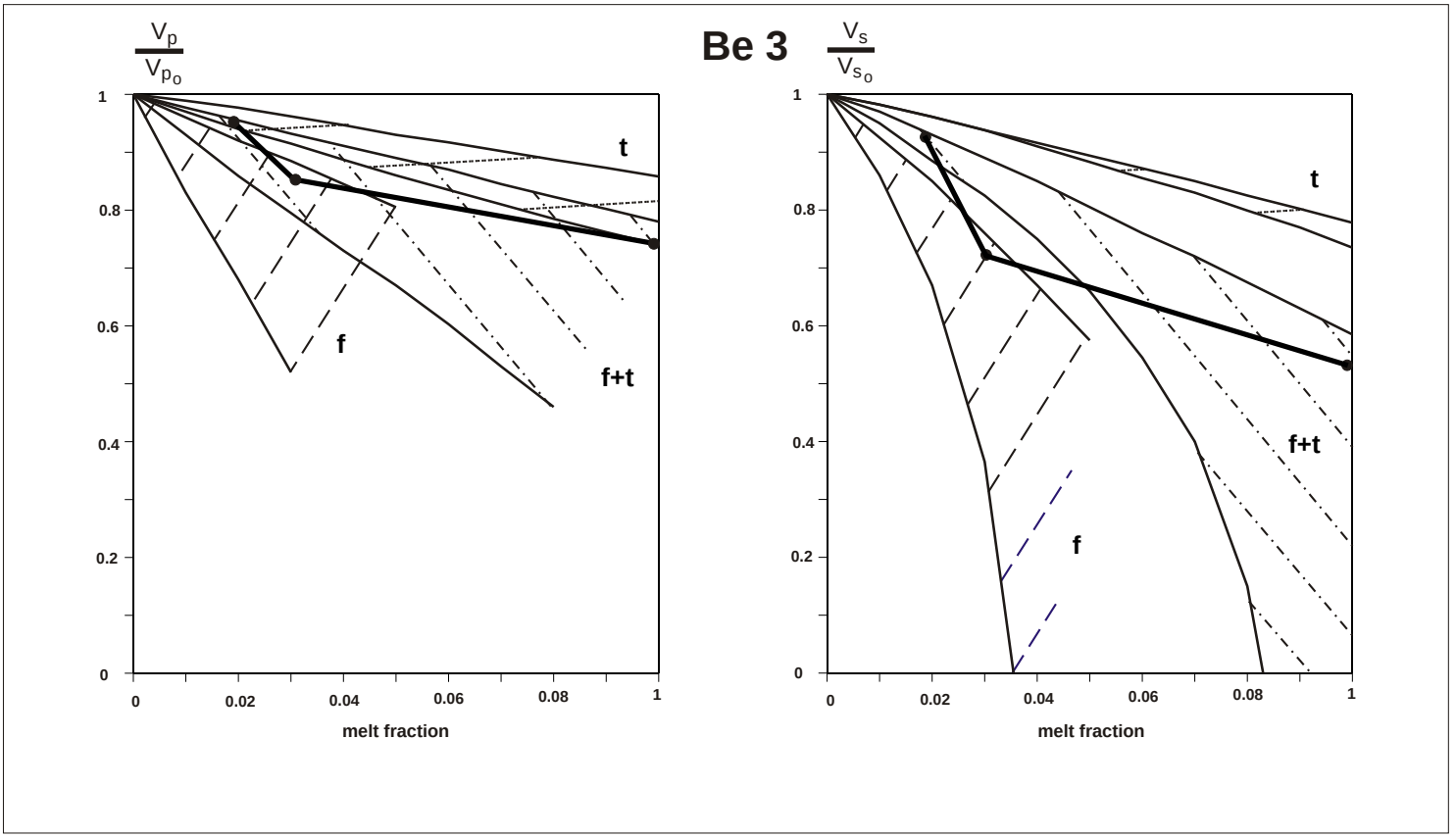

Fig. 8: Relation between melt content, melt distribution and the elastic wave velocities v_p and v_s (modified from Mavko, 1980 and hp-hT data of this work)

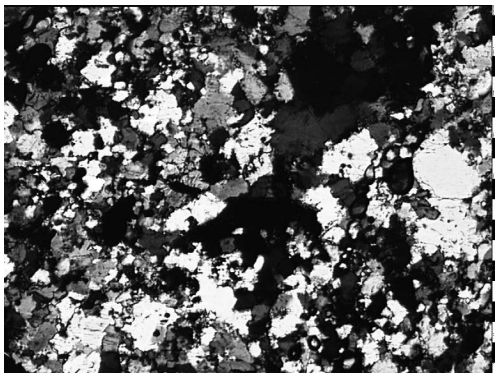

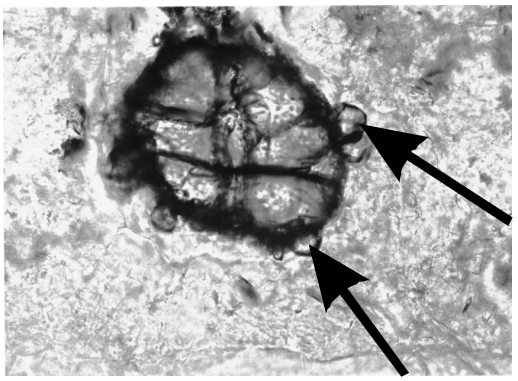

postexperimental state **new formed garnet**

Mineral content: gnt (old), gnt (new), plg (old), kfs (new), quartz, opx (new), apatite

Fig. 9: Structure creation during petrophysical long-term high-p-T experiments - 1.5 GPa, 850°C, 48 h

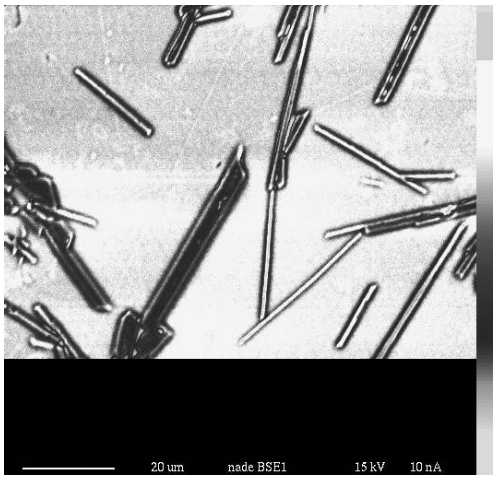

new formed corundum in melt
BSE-image, color coded,
image diagonal 100 µm

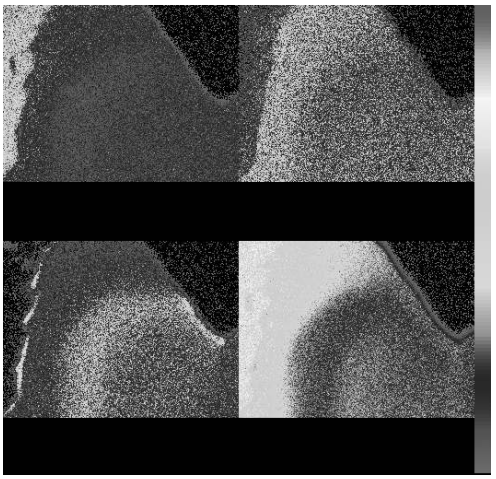

element partitioning in melt structures
granite Be 3
image diagonal 60 µm

Fig. 10: Structure creation during petrophysical long-term high-p-T experiments
- 0.5 GPa, 1,200°C, 48 h

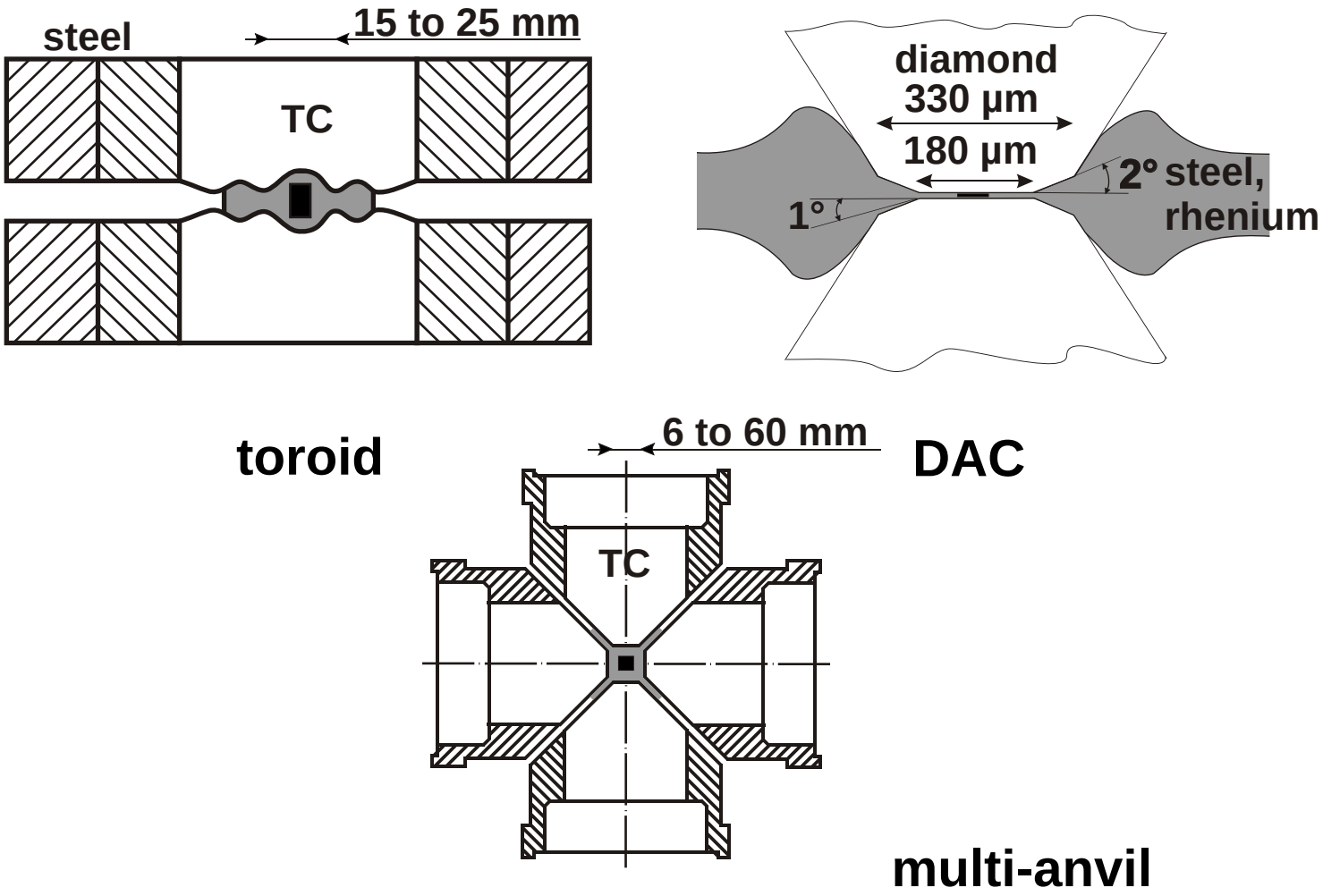

Fig. 11: Experimental simulation of mantle conditions with synchrotron radiation access

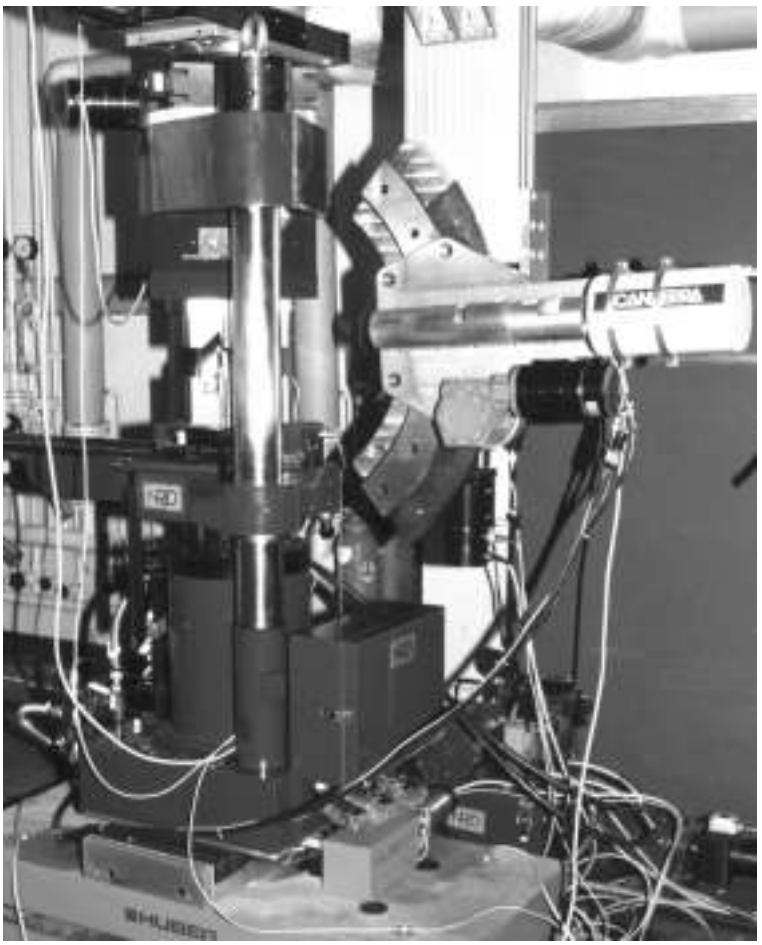

Fig. 12: Double- and single-stage multi-anvil DIAs
- MAX 200x - 1750 tons
- MAX 80 - 300 tons

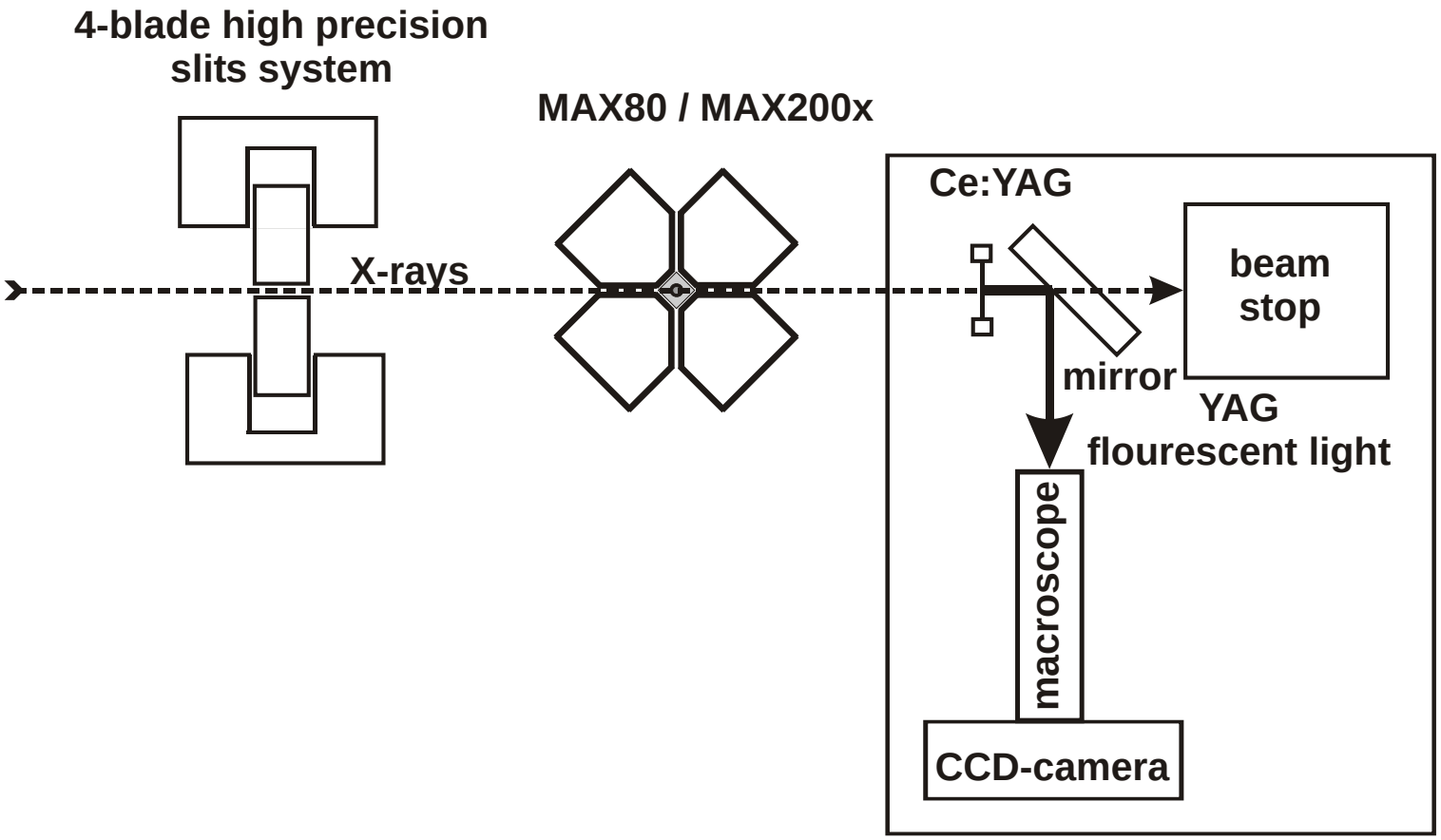

Fig. 13: X-Radiography scheme for in situ deformation measurement

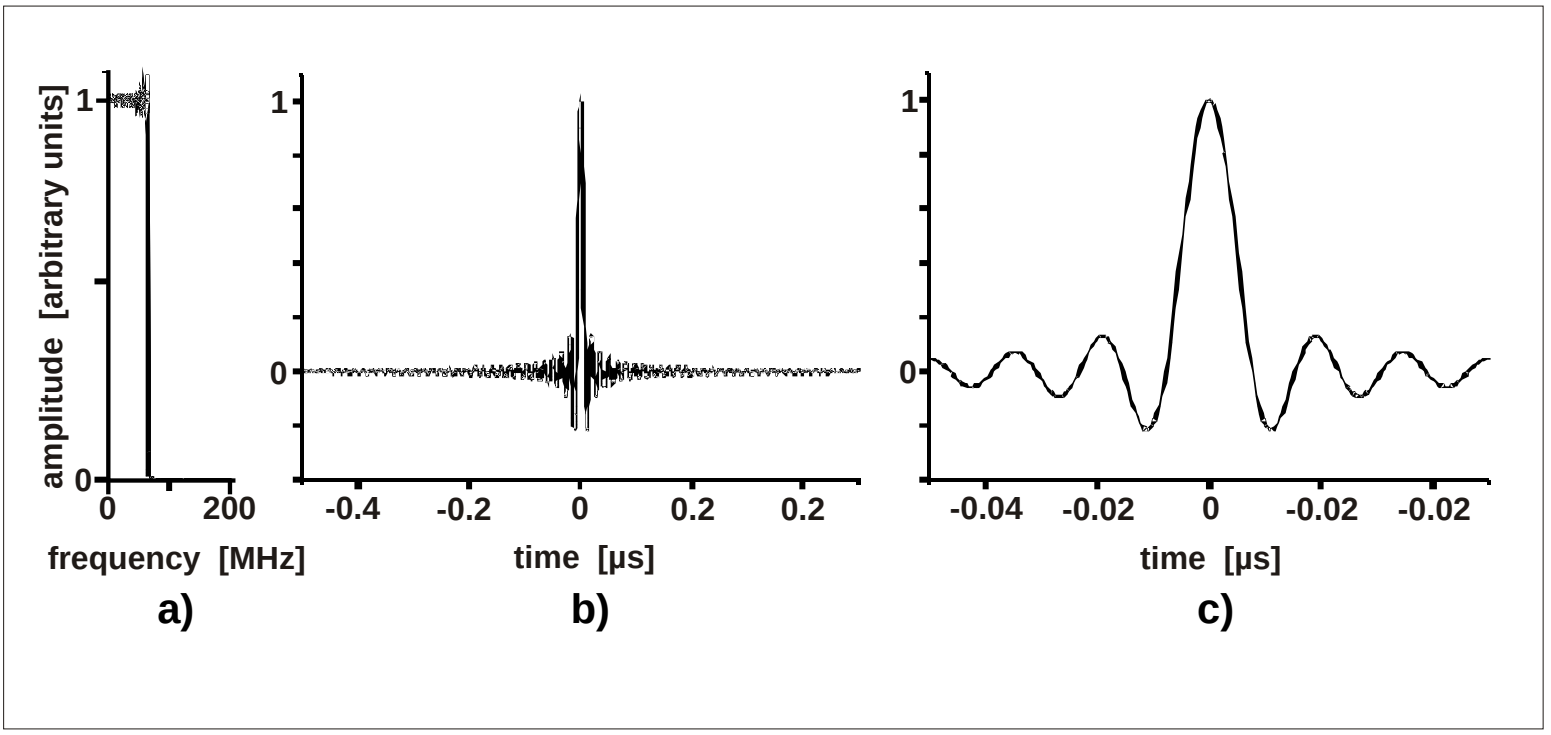

Fig. 14: DTF-technique: Excitation function with a cut-off frequency of 65 Mhz
a) FFT
b) time base: 1 µs
c) time base: 0.1 µs

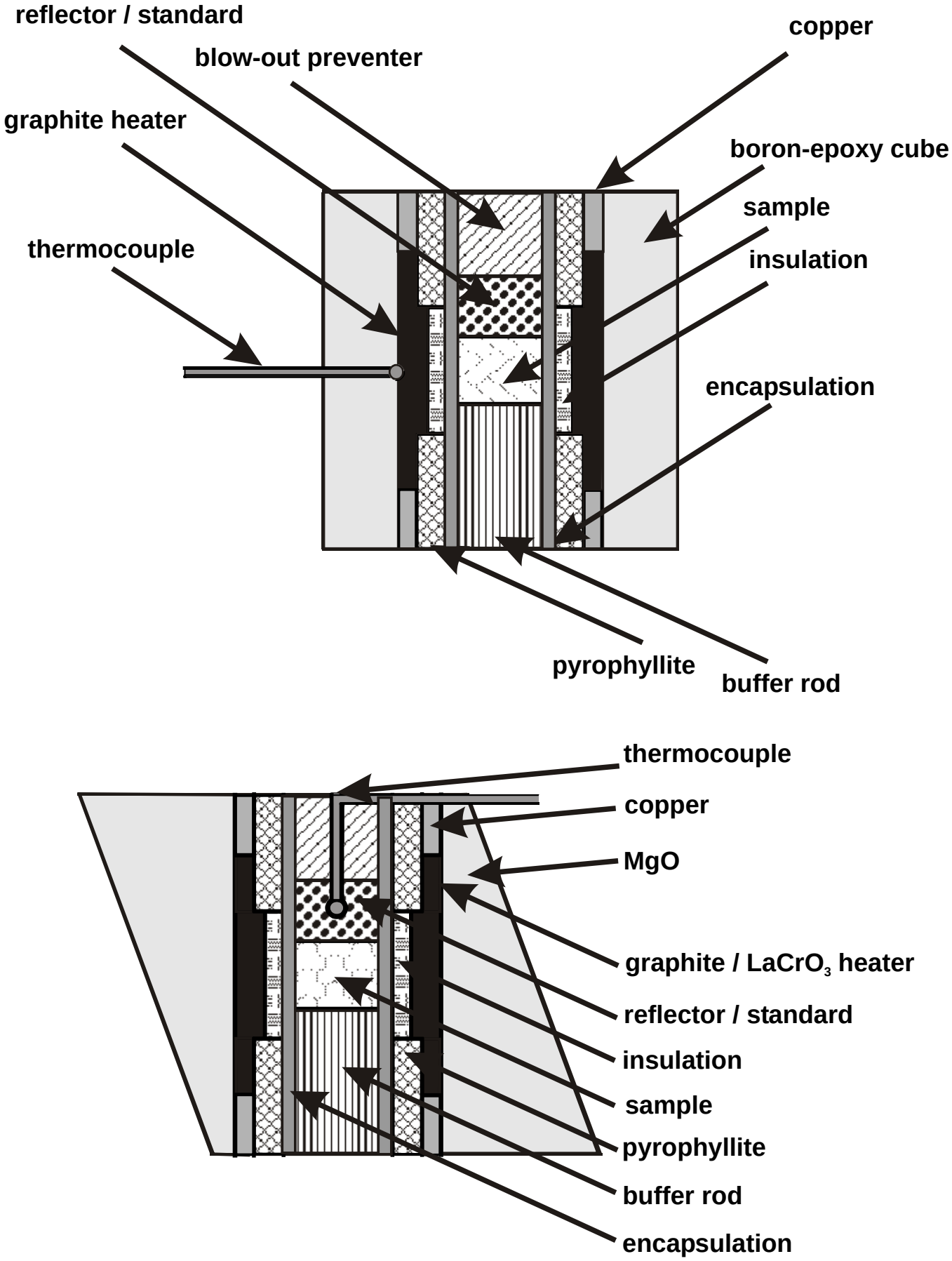

Fig. 15: Encapsulated sample ultrasonic set-up for MAX 80 - single-stage DIA (top) and for MAX 200x - double-stage DIA (bottom)

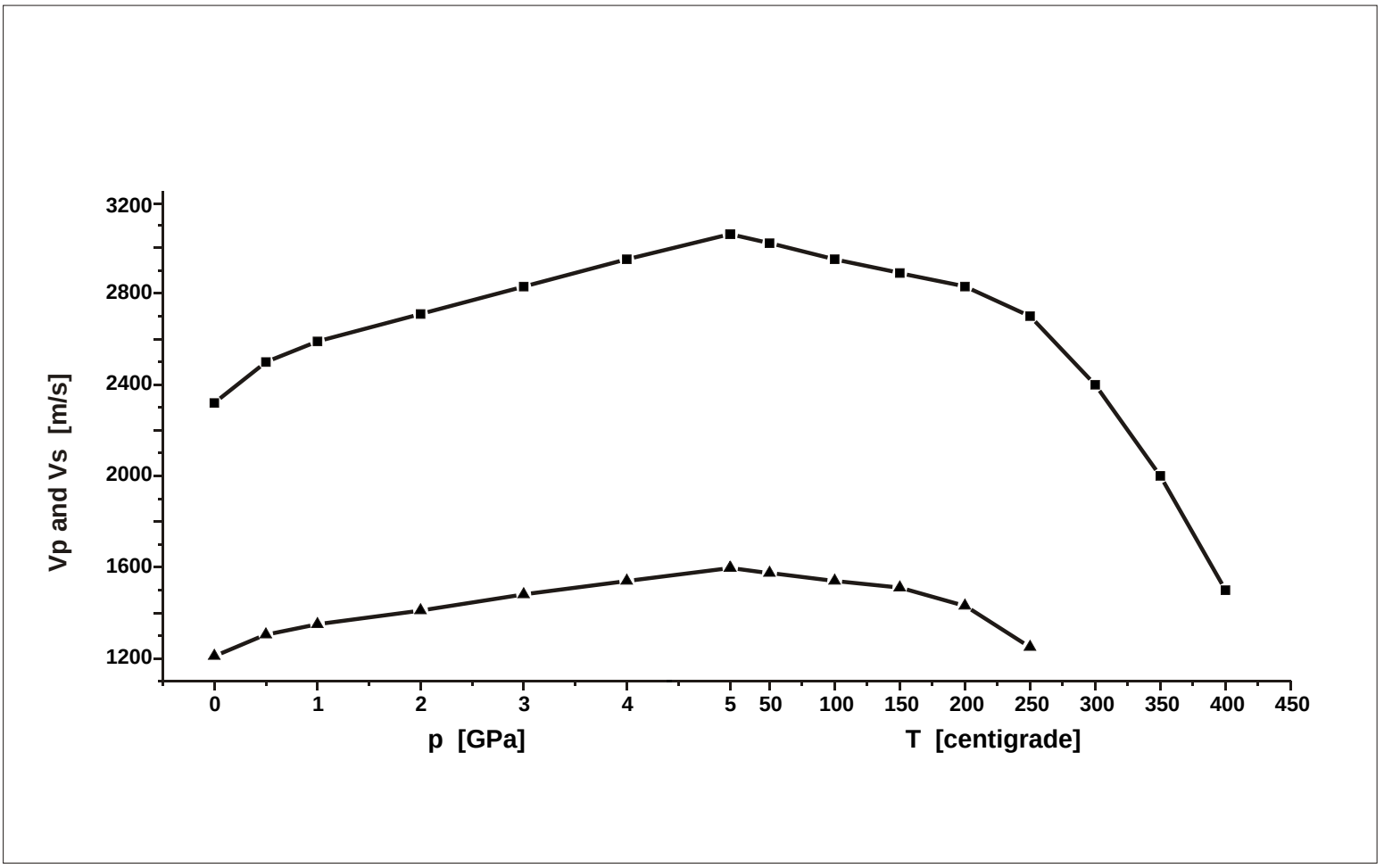

Fig. 16: v_p and v_s for thermo-plastical lute up tp 0.5 GPa and 400°C

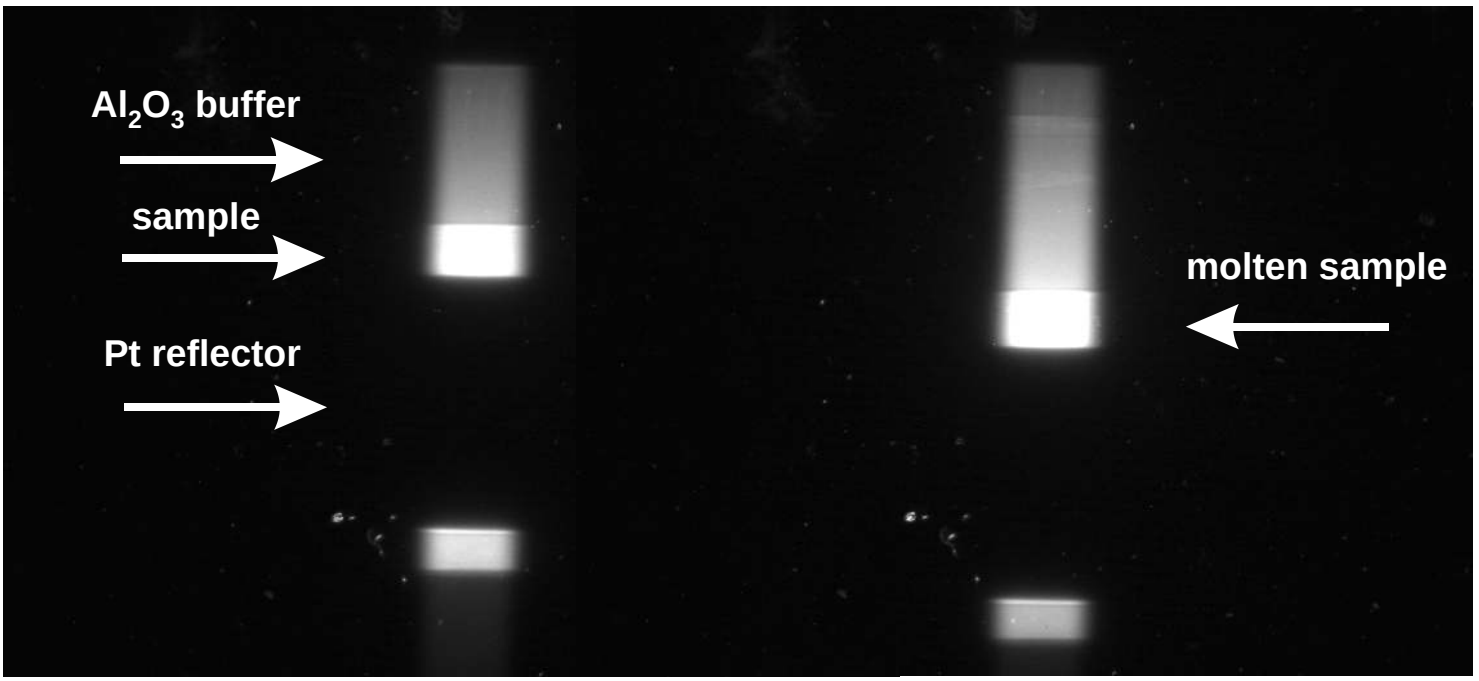

Fig. 17: X-Radiography of an encapsulated ultrasonic sample before and after melting under high pressureat 0.5 GPa

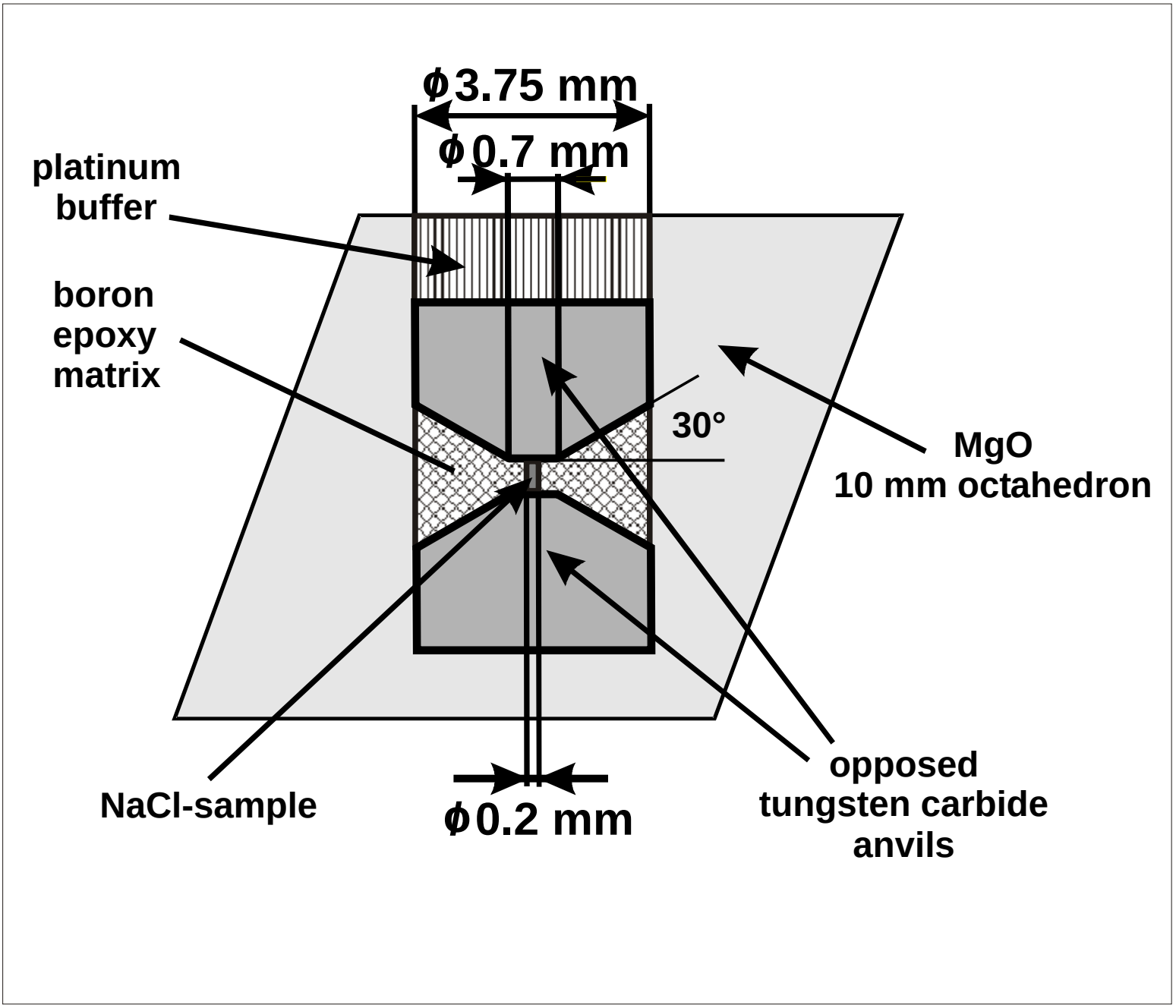

Fig. 18: Triple-stage opposed anvil ultrasonic set-up